The Development of Functional Mesocrystals for Energy Harvesting, Storage, and Conversion

Zhang, Peng
Tachikawa, Takashi
Fujitsuka, Mamoru
Majima, Tetsuro

(Citation)
Chemistry - A European Journal,24(24):6295-6307

(Issue Date)
2018-04-25

(Resource Type)
journal article

(Version)
Accepted Manuscript

The Development of Functional Mesocrystals for Energy Harvesting, Storage, and Conversion

Peng Zhang[a], Takashi Tachikawa*[b,c], Mamoru Fujitsuka[a], and Tetsuro Majima*[a]

Dedication ((optional))

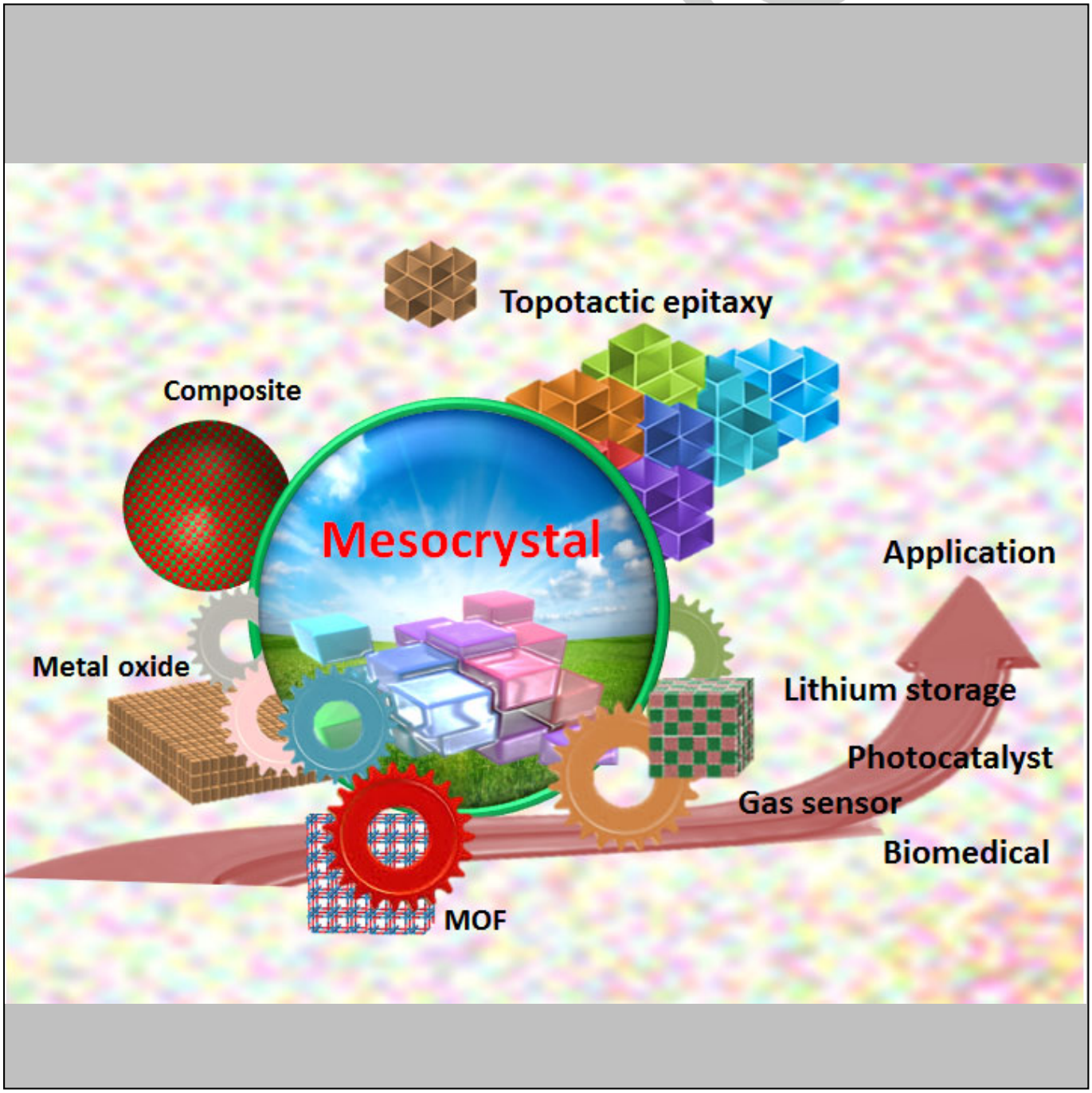

Abstract: Higher-ordered semiconductors have attracted extensive research interest as an adopted engineering for active solar energy harvesting, storage, and conversion. It is well-known that the effective separation and anisotropic migration of photogenerated charges are the basic driven force required for superior efficiency. However, the morphology and stoichiometric variation of these semiconductors play essential roles in their physicochemical properties of bulk and surface, especially for efficient interparticle or interfacial charge transfer. To this point, the strategy of controlling the topotactic transformation toward superstructures with optimized functionality is preferable for a wide range of optoelectronic and catalytic engineering applications. In this review, we provide an overview of the crystal orientation, synthetic engineering, functional applications, and spatial and temporal charge dynamics in TiO_2 mesocrystals and others. The viewpoint of in-depth understanding of the structure-related kinetics would offer an opportunity for design of versatile mesocrystal semiconductors sought-after for potential applications.

1. Introduction

Mesoporous materials have been attracting intense research and technological interest in the wide-ranging applications from (photo)catalysts to batteries and electronics.[1] It is well-known that the conventional physical and chemical properties of materials are dominated by their crystallographic constitution and periodic nanopores and atomic lattices.[2] The exceptional features of mesoporous materials are available for encompassing and improving the performance in terms of efficiency, lifetime, and stability. The high surface areas provide more active sites for adsorption and catalysis, while tunable pore sizes and shapes are beneficial for efficient loading of specific guest species.[3] Furthermore, the uniform mesochannels would largely facilitate the atoms, ions, and large molecules accessing to active sites through the bulk of the material. It means that the assembly of ordered mesopores in crystal can improve their intrinsic properties through the intimate connectivity.[4] State of the art, the controllable synthesis of hierarchical structures with dense packing of nanocrystals can enhance the active performance of dye-sensitized solar cells.[5] It has been suggested that the mesoporous TiO_2 consisting of regularly-ordered nanoparticles significantly enhanced charge transport and recombination, owing to the efficient interparticle electron transfer.[5c, 5g, 5h] Although the above-mentioned systems have succeeded in promoting the reaction behaviors, it is becoming urgent to design of high-quality superstructures with superior performance for practical applications.

From this point of view, we found that the hierarchical mesocrystals with ordered and mesoporous structures, mainly originated from the lattice structure and scale of the parent templates, offer principal opportunities in desirable applications owing to their extraordinarily high surface areas, good crystallinity, and efficient anisotropic charge migration.[6] From the pioneering concept of Cölfen, a mesocrystal was defined as a mesoscale assembly of nanoparticle building blocks for substituting the single-crystalline or porous polycrystalline materials.[6-7] It was proposed that the particle-mediated mesocrystal growth (bottom-up route) involves a non-classical crystallization process (Figure 1, the red route), which is different from the classical mechanism of atom/ion-mediated growth (Figure 1, the blue route).[6d] The four principal possibilities were mentioned here to explain the oriented alignment of nanoparticles in building blocks (Figures 1a-1d). In addition, topotactic reactions (top-down route) as the alternative way are often developed for the preparation of mesocrystals (Figure 1, the green route). In both cases, the hierarchical superstructures represent the typical properties of mesocrystals. Another definition of the “mesocrystal” should be noted here that its sole criterion is determined from the unique crystallographically hierarchical structure instead of its formation mechanism even in metastable or amorphous case.[8] Up to now, an increasing number of representative mesocrystals was developed involving metal oxides,[9] metal chalcogenides,[10] noble metals,[11] organic compounds,[12] fullerene,[13] and so on. With the increasing consideration on mesocrystals, it is essential to readily access the commercial application attributed to their abundant physicochemical properties.

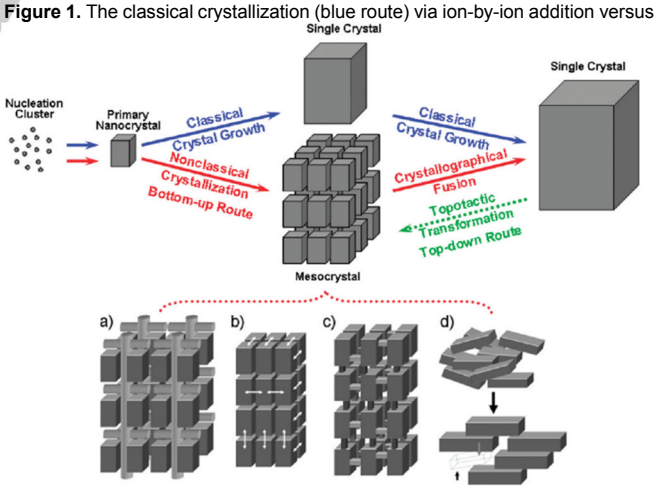

Figure 1. The classical crystallization (blue route) via ion-by-ion addition versus single-crystal formation (red route) by a mesocrystal intermediate made of nanoparticles. (a−d) Illustrative diagrams of the four principal possibilities that could explain the 3D oriented alignment of nanoparticles, (a) by an oriented organic matrix, (b) by physical fields or mutual alignment of identical crystal faces, (c) by epitaxial growth of a nanoparticle employing a mineral bridge connecting the two nanoparticles, and (d) by nanoparticle alignment by spatial constraints. Figure reproduced with permission from ref. [6d]

[a] Dr. P. Zhang, Prof. M. Fujitsuka, Prof. T. Majima
The Institute of Scientific and Industrial Research (SANKEN)
Osaka University
Mihogaoka 8-1, Ibaraki, Osaka 567-0047 (Japan)
E-mail: majima@sanken.osaka-u.ac.jp
[b] Prof. T. Tachikawa
Molecular Photoscience Research Center
Kobe University
1-1 Rokkodai-cho, Nada-ku, Kobe 657-8501 (Japan)
[c] Prof. T. Tachikawa
PRESTO, Science and Technology Agency (JST)
24-1-8 Honcho Kawaguchi,Saitama 332-0012 (Japan)

In this review, we highlight the procedure of topotactic reaction in recent developments of mesocrystals and overview various aspects in energy conversion and storage and environmental fields. Especially for TiO_2, we discuss the anisotropic charge migration based on the fundamental characterizations by conductive atomic force microscopy (AFM), single-molecule, single-particle fluorescence microscopy, and time-resolved diffuse reflectance (TDR) spectroscopy, clearly unveiling the structure-related superior performance. The well-defined mesocrystals with tunable morphologies and sizes remain a research focus and a challenging issue in future investigation. However, it is believed that the topotactic transformation can serve as a promising route and make the continued efforts in scope of mesocrystal for potential application.

Peng Zhang received his M.S. degree form Shanghai Normal Univeristy in 2012. In 2016, he received the Ph.D. degree under the supervision of professor Tetsuro Majima at SANKEN, Osaka University. From 2016, he worked as the specially-appointed assistant professor in SANKEN. His research interests are in the areas of temporal and spacial resolved charge transfer dynamics and development of mesocrystals for energy and environmental applications.

Takashi Tachikawa received his Ph.D. in Chemistry from Tohoku University in 2003. He worked as a postdoctoral fellow, the specially-appointed assistant professor, and assistant professor at SANKEN, Osaka University until 2014. Now he is an associate professor in Kobe University. He was also a researcher of the PRESTO (JST) program from 2013 to 2017. His scientific interests include the photochemical processes and energy conversion at the single-molecule, single-particle level.

Mamoru Fujitsuka received his Ph.D. from Kyoto University in 1994. After two years work as a postdoc, he joined the Institute for Chemical Reaction Science, Tohoku University, as a research associate in 1996. In 2003, he moved to SANKEN, Osaka University, as an associate professor. His scientific interests include the photoexcitation dynamics of functional molecules.

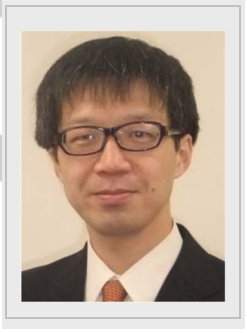

Tetsuro Majima received his Ph.D. from Osaka University in 1980. He worked as a research associate in the University of Texas at Dallas for two years (1980–1982) before moving to RIKEN, Japan. In 1994 he moved to SANKEN, Osaka University, as an associate professor. He was promoted to a full professor in 1997. His current research interests include photochemistry of supramolecules, DNA, protein, metal nanoparticles, and photocatalysts.

2. Versatile topotactic reactions

In recent years, the promise development of mesocrystals with heterostructures has received considerable attention in wide field of applications.[6-7] Referred to the definition of Cölfen,[6-7] final mesocrystals are constructed through the topotactic transformation among single crystal particles or intermediate phases, retaining the unique memory of the initial morphology. There is an immense interest in potential design of mesocrystals with hierarchical structures in critical dimensions. To this end, versatile topotactic reactions are essential for design of a variety of mesocrystals with desired ordering morphology and crystallographic alignment of nanoscale building blocks.

2.1. Topotactic transformation in prototype TiO_2

Since 1972,[14] TiO_2 has been extensively studied due to its low cost, environmental friendliness, and potential applications in wide fields.[5] To the best of our knowledge, the higher-order structures of semiconductor-based photocatalysts play crucial roles in their physicochemical properties for efficient solar-energy conversion. It is thus crucial to seek a versatile route for the structure and property design of TiO_2 superstructure with a regular shape and uniform size. There are various methods to successfully synthesize TiO_2 mesocrystals in the past decades.[9a, 9e,15] Originally, O'Brien et al. obtained the anatase TiO_2 mesocrystal via the topotactic transformation from NH_4TiOF_3 crystals.[9a] It was revealed that the mesocrystal growth is a non-classical crystallization (Figure 2, upper). During the transformation, the NH_4TiOF_3 mesocrystal provided a crystallographically matched template for the oriented transformation and subsequent growth of the TiO_2 mesocrystals due to their similar critical parameters[16] with less than 0.02% in an average lattice mismatch.[9a] The crystallographically equivalent and orientational relationship between two materials on the {001} planes was in line with the corresponding selected area electron diffraction (SAED) patterns (Figure 2, bottom). After that, the TiO_2 mesocrystals with layered structure were successfully prepared.[9c] Mostly, the earlier reports on TiO_2 mesocrystals were based on the oriented transformation from NH_4TiOF_3 due to the difficulty in direct growth.[15e, 15f] To this end,

a series of tailored mesocrystals in the phase of anatase or rutile[17] were published via facile hydrothermal/solvothermal reaction with[18] or without additives.[15b, 15d, 19] In 2012, Bian et al. published the one-step annealing process to synthesize TiO_2 mesocrystal with dominant facets of {001} via topotactic transformation from intermediate NH_4TiOF_3.[9e] The constructed porous building blocks assembled with ordered alignment of anatase nanocrystals remarkably result in long-lived charges, better photoconductivity, and higher photocatalytic activity, which will be discussed in section 3. [9e, 20] Topotactic conversion is a meaningful way to construct mesocrystals. For another example, the unique morphology of MnO_x was manipulated after topotactic transformation from its precursor of metal carbonates ($MnCO_3$) for potential application in adsorption, catalysis, and electrochemical storage.[21]

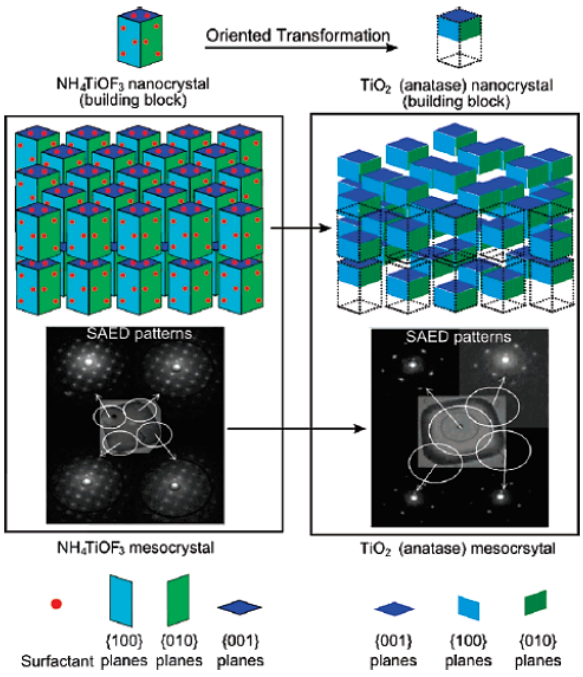

Figure 2. Illustration of the oriented transformation of TiO_2 (anatase) mesocrystal from NH_4TiOF_3 mesocrsytal. Figure reproduced with permission from ref.[9a]

2.2. Topotactic transformation in composite mesocrystal

It is well known that the efficient charge separation would occur between n-type (e.g., TiO_2 and ZnO[9h-r]) and p-type (e.g., CuO[9ab-ad] and NiO[22]) semiconductors than single phase. From this viewpoint, a general preparation of composite mesocrystals was achieved via a facile mixing of different metal precursors (Figures 3a and 3b).[23] By gradual annealing, seed nanoparticles are self-assembled with capping agent (e.g., Pluronic P123 polymer) and attached together to form intermediate crystals with specific morphologies. Finally, the composite mesocrystals of metal oxides were obtained from the intermediate crystals through the topotactic transformation, while maintaining their morphologies. The internal distribution of ZnO and CuO nanocrystals in the composite mesocrystal was investigated, where an ultramicrotome was used to section the mesocrystals. The analysis of high-resolution elemental mapping visualized that ZnO and CuO nanocrystals inside the mesocrystal are intimately contacted (Figures 3c-3f). The ultrafast dynamics of interfacial charge transfer betweeen ZnO and CuO was further clarified from the significant photoluminescence (PL) quenching and charge accumulation by means of the time-resolved spectroscopies. It was believed that the facilitation of the interfacial charge transfer between the nanocomposite mesocrystalline heterostructures is preferable for their widely applications among the field of photovoltaics and photocatalysis.[24]

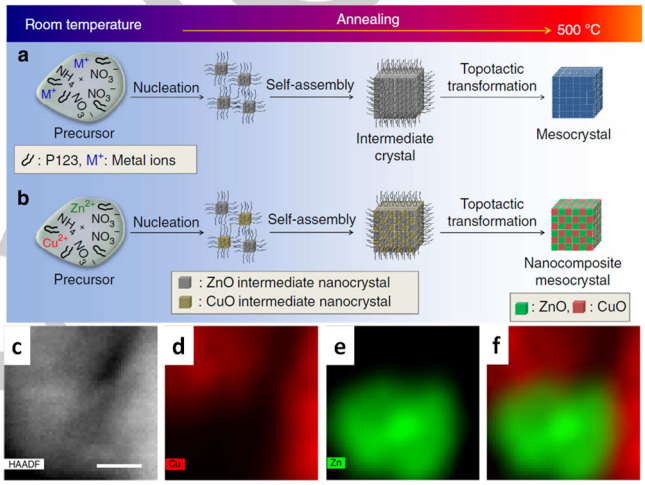

Figure 3. The formation mechanisms of metal oxide mesocrystals. (a) Single-metal element (for example, ZnO, CuO, NiO and TiO_2) and (b) nanocomposite mesocrystals. (c) High-resolution cross-sectional HAADF-STEM image of ZnO-CuO mesocrystal and elemental mapping images of Cu (d) and Zn (e), and merge image (f). Scale bar, 10 nm. Figure reproduced with permission from ref.[23]

2.3. Topotactic transformation in polymerization

Furthermore, topotactic transformation with utility and flexibility is a feasible approach to fabricate versatile materials, such as CoZn hydroxides, porous metal phosphates, metal organic frameworks (MOF), and so on.[16, 25] In the case of transition-metal nitrides, a series of graphene-encapsulated $Fe_xMn_{6-x}Co_4$-N@C ($0 < x < 6$) with well-inherited morphology by topotactic transformation from MOF was obtained in N_2 atmosphere.[26] During the thermal decomposition, Co and Fe atoms form as the FeCo alloy, and Mn atoms as Mn_4N nanocrystals inside, attributed to the same crystal system (cubic) and space group (Pm-3m) of FeCo and Mn_4N (Figure 4a). Using the CN^- groups of prussian blue analogues (PBAs) as nitrogen and carbon sources to form nitrogen-doped graphene layers, the construction from the small FeCo and Mn_4N nanocrystals was encapsulated in graphene layers. With increasing of Mn content, a regular change of the morphology of dice-like structure is realized (Figures 4b-4e). To this point, the efficient catalytic

degradation of bisphenol A is in accordance to the dramatically reduced adsorption energy and facilitated electron transfer for peroxymonosulfate activation by Mn_4N. It should be noted that the topotactic transformation of engineered monomer crystals has received considerable attention in recent years as polymerization and reversible polymerization methods leading to stereoregular chain structures.[27]

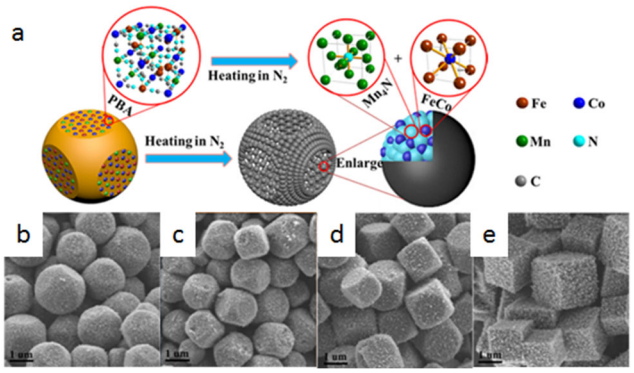

Figure 4. The model of the graphene encapsulated $Fe_xMn_{6-x}Co_4$-N@C in preparation route (a) and well-controlled morphology (b-e). Figure reproduced with permission from ref.[26]

2.4. Topotactic transformation in epitaxial growth

Epitaxial growth, referred to the oriented deposition of a crystalline material over another crystalline substrate, can be applied to synthesize different crystal structures on the substrate material. It would be highly desirable to extend this strategy to directly fabricate new mesocrystals with hierarchical structures. With the development of topotactic transformation, topotactic epitaxy as the novel reproducible strategy, orientating from the initial mesocrystal, was extensible as nonlithographic method for design of various bismuth compound[28] and perovskite structure recently.[29]

Among bismuth semiconductors, a series of BiOX (X = Cl or Br), Bi_2O_3 and Bi_2S_3 with promising architectures of nanowall and network are attracting considerable interest in the field of electronic devices and photocatalysts.[28] To this point, Liu et al. provided lattice-directed nonlithographic superstructure, involving the anisotropic nucleation from intermediate BiOCl (Br) to Bi_2S_3 based on topotactic transformation.[28a] As presented in scanning electron microscopy (SEM) image (Figure 5a) and schematic illustration (Figure 5b), the two dimensional orthogonal networks (2DONWs) of BiOCl nanowall (tetragonal structure, a = 3.887 Å and c = 7.354 Å) epitaxially grow in the perpendicular direction from β-Bi_2O_3 film (tetragonal structure, a = 7.741 Å and c = 5.634 Å) in diluted hydrochloric acid (HCl). After that, the BiOCl nanowall transforms to Bi_2S_3 network of nanorods with the presence of S^{2-} (Figure 5c). These superstructures are formed by the preferential growth of [001]-oriented Bi_2S_3 nanorods on the top faces of (001)-oriented BiOCl along the two perpendicular [100] and [010] directions of BiOCl, attributed to the close matching between their lattice constants. Similar to BiOCl, the BiOBr (tetragonal structure, a = 3.927 Å and c = 8.101 Å) 2DONW (Figure 5d) can also transform to nested self-similar 2D orthogonal networks (N2DONWs) of Bi_2S_3 nanorods (Figure 5e). Also, it was interesting to conduct the epitaxial growth of AgCl crystals on BiOCl after ion-exchange reactions during the topotactic transformation, i.e., orientation ordering with the (001)BiOCl||(100)AgCl crystallographic relationship.[30] The extendable bismuth compounds with attractive technological properties will show good promise for practical applications in electronic devices, sensors, and photocatalysts.

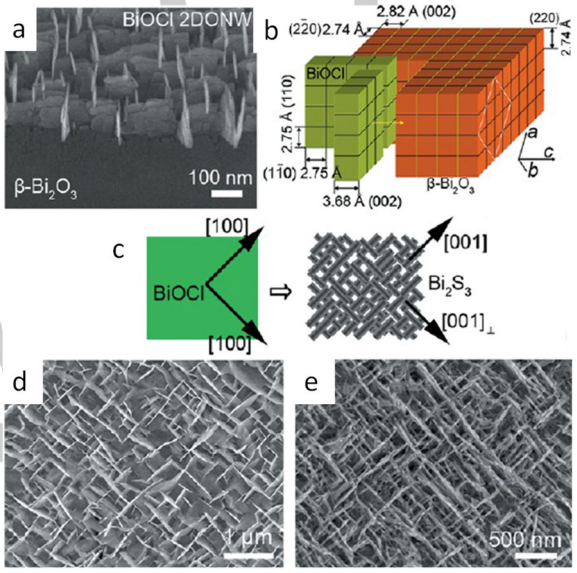

Figure 5. (a) Tilt view of a BiOCl 2DONWs grown from β-Bi_2O_3. (b) Schematic illustration on the epitaxial relationship between BiOCl nanowalls and β-Bi_2O_3 and (c) subsequent transformation between BiOCl nanowall and Bi_2S_3 network. SEM images of epitaxial BiOBr (d) and its transformation product of Bi_2S_3 (e). Figure reproduced with permission from ref.[28a]

The perovskite strontium titanate ($SrTiO_3$) mesocrystal superstructures with well-defined orientation of assembled cubic nanocrystals were synthesized by topotactic epitaxy from TiO_2 mesocrystals.[29a] During the crystallographic epitaxy between the anatase and perovskite structures in alkaline hydrothermal growth, OH^- will neutralize H^+ adsorbed on the O-terminated {001} facets of the TiO_2 mesocrystals, leading to growth along the [001] axis and exposure of the dominant {100} facets on the $SrTiO_3$ mesocrystals (Figure 6a).[29b] The chemical bonds formed at the interface of TiO_2/$SrTiO_3$ from the structural distortion of TiO_6 octahedra are assumed to be important in determining the final phase of the perovskite structure.[31] The resulting orientation is the [001] axis of anatase being parallel to the [100] axis of $SrTiO_3$, because of the very small in-plane lattice mismatch between $SrTiO_3$ (cubic crystal, a = 0.39 nm) and TiO_2 (tetragonal crystal, a = b = 0.38 nm, c = 0.95 nm) of around 3%.[29a] As a prototypical ABO_3-type perovskite, $SrTiO_3$ mesocrystal is attracting growing attention and applied in the fields of electromagnetic devices [32] and solar energy conversion systems.[33] A similar solution-mediated topotactic transformation from $H_{1.08}Ti_{1.73}O_4$ to $BaTiO_3$

was reported by Feng et al.[34] Here, Ba^{2+} ions can migrate into the crystal bulk through the interlayer pathway and react with the TiO_6 octahedral layers of $H_{1.08}Ti_{1.73}O_4$ in the crystal bulk to form $BaTiO_3$ in site.[34] Simultaneously, the topochemical molten salt synthesis promoted as one of the strategic approaches to prepare functional perovskite structure with dimensional morphology and pure phase.[35] To design such hierarchical materials with visible-light response, the labile hydride strategy of topotactic reaction is becoming an alternative way for appropriately bandgap narrowing. Kageyama et al. developed topochemical nitridation,[29c, 36] i.e., anion diffusion to reach the terminal oxynitride started from perovskite $BaTiO_3$, in which the lability of H^- in the oxyhydride allows H^-/N_3^- exchange to occur by low-temperature ammonolysis to yield $BaTiO_{3-x}N_{2x/3}$ via mixed O–H–N intermediates (Figure 6b). Therefore, the topotactic transformation with facile energy level modulation is rapidly expanding in scope of design efficient visible-light response photo(electronic)catalysts of various oxynitride and even a large number of mixed anionic transition metal oxides with versatile morphologies.

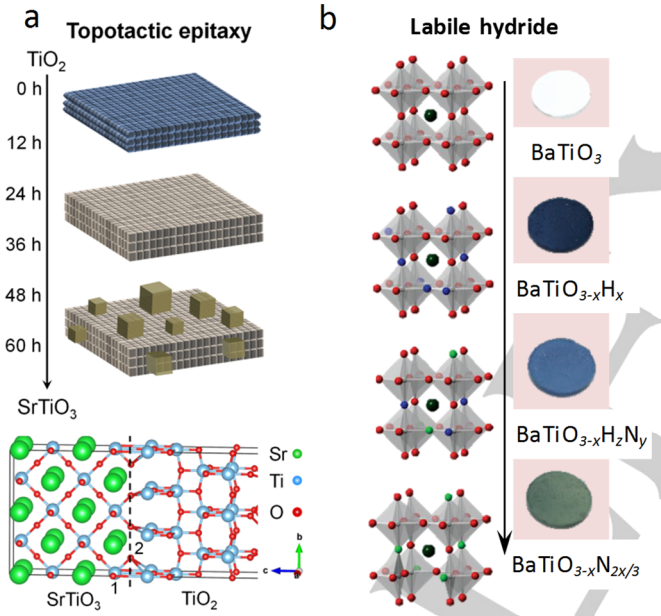

Figure 6. (a) Topotactic epitaxy of $SrTiO_3$ mesocrystals from TiO_2 mesocrystals and their interface structure. (b) Synthesis of oxynitride $BaTiO_{3-x}N_{2x/3}$ from $BaTiO_3$ via the oxyhydride–nitride. Figure reproduced with permission from refs.[29b] and [36]

3. Anisotropic charge separation in mesocrystal

With the prospect of further reducing human energy usage and alleviating environmental pollution, it is still one of the key and prominent topics to design the alternative superstructures in terms of efficient charge separation and remarkable long-lived charge carriers for boosted active performance. Choi et al. revealed that the mesoporous TiO_2 with aligned nanoparticles exhibited superior photocatalytic hydrogen evolution than commercial TiO_2.[5c] As a new class of nanostructured solid materials, an increasing number of metal oxide mesocrystals, such as TiO_2,[9a-d, 9f, 9g] ZnO,[9h-r, 37] Fe_2O_3,[9s-v],[38] CeO_2,[39] NiO,[22] Co_3O_4,[40] WO_3,[41] VO_2,[42] and CuO,[9ab-ad] was developed through different ways.[6, 7c, 9aa, 9ad, 38a] Beyond the characterization of structures and the investigation of formation mechanisms, the importance of interaction between aligned nanoparticles is still poorly understood. Interestingly, it was recently highlighted that TiO_2 mesocrystals (TMCs), the superstructure assembled by oriented anatase TiO_2 nanoparticles, exhibited superior electron transport properties than disordered systems by conductive AFM.[9e, 43] The superstructures with tunable morphologies[44] further provided the in-depth understanding of the favorable behavior on exposed facets.[45] To clarify the superstructure-dependent activity, we investigated their structural and optoelectronic characterizations by the means of single-molecule, single-particle fluorescence microscopy for unraveling the charge transport and photocatalytic properties of individual crystal, and TDR spectroscopy for monitoring the charge transfer dynamics.

3.1. Conductive atomic force microscopy

It is well known that the aggregates of TiO_2 nanoparticles (disordered system, Nano) with higher surface area typically present numerous interfacial disorders for undesirable charge recombination.[5b] When compared to the poor performance of interparticle charge transfer in disordered system,[5c-f] the ordered nanocrystalline structure exhibited considerably improved charge transport process.[5g, 5h] The TMCs, well-ordered superstructures composed of anatase nanocrystal building blocks, exhibited promising activities due to their paramount improvement in interfacial charge transfer dynamics.[9e] It is important to clarify the intricate relationship of photoinduced charge transfer between structure and function on individual TMCs via the photoconductivity measurements with conductive AFM (Figure 7a).[9e] The platinum AFM tip was used to measure the surface topography and photocurrent under bias potential. The typical AFM images of TMC (upper) and Nano (lower) on indium tin oxide (ITO) electrode are shown in Figure 7b. The measured current-voltage curves from the marked point indicate the different efficiency of electron injection from platinum and ITO into the different TiO_2 system. It was found that there is a primary effect of thickness of TMCs on photocurrent generation (Figure 7c). It is interesting that the photocurrent attained maximum 0.5 nA at lower UV intensity in TMC than Nano, attributed to the intimate contact between nanocrystals. From the calculation of photocurrent at the same thickness (~200 nm), the photoconductivity of TMCs (2×10^{-2} Ω^{-1} m^{-1}) was much greater than that of aggregated system in air (Figure 7d, inset), suggesting the improved electron transport ability between adjacent nanocrystals and electrodes. From the PL quenching, metal/TMC has larger electron transport distance and electron diffusion coefficient, again emphasizing the importance of interparticle charge transfer among the ordered alignment of nanocrystals in mesocrystals.[20]

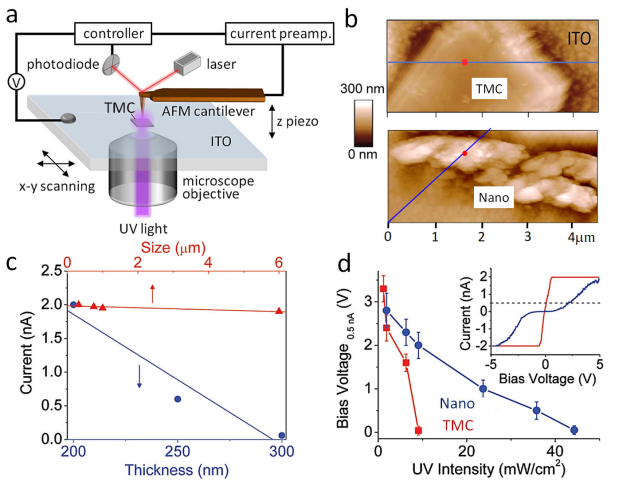

Figure 7. (a) The schematic of photoconductive AFM equipped with an inverted fluorescence microscope. (b) Topological image of TMC and Nano on ITO. The red dot indicates the location where current–voltage curves was measured. (c) Size and thickness dependence on the photocurrent observed for TMC. (d) Response voltages achieving a current of 0.5 nA, plotted against UV intensity. The inset shows the comparison of typical current–voltage curves between TMC and Nano. Figure reproduced with permission from ref.[9e]

3.2. Single-molecule, single-particle spectroscopy

It was clearly revealed that the long-range ordered TMCs significantly retard the charge recombination due to the anisotropic electron flow in the network.[20] With modification of co-catalysts, rapid and efficient collection of photogenerated electrons or holes on the catalytic sites is of paramount importance in the entire reaction. To this point, single-molecule, single-particle fluorescence microscopy has been selected as a powerful tool to determine the spatial distribution of the redox sites on individual TMCs by using a redox-responsive fluorogenic probe. [20, 46] Figure 8a shows a typical total internal reflection fluorescence (TIRF) image of 0.04 wt% Au-loaded TMC (Au/TMC) in Ar-saturated 3,4-dinitrophenyl-BODIPY (DN-BODIPY) under both 488 nm laser and UV light irradiations. The single-molecule fluorescence signals (arrowed parts) from 4-hydroxyamino-3-nitrophenyl-BODIPY (HN-BODIPY) were clearly observed after the reduction of DN-BODIPY by accepting electrons from photoexcited TiO_2 (Figure 8b). As shown in Figure 8c, it was found that more fluorescence spots were located near the lateral faces of individual Au/TMC (bottom) than TMC (top); this result is in line with the preferential photodeposition of noble metals (Au or Pt) at the edges of TMC.[38a] Note that the difference was due to the fact that photogenerated electrons on the basal surfaces of TMCs can preferentially migrate to Au nanoparticles loaded on the lateral {101} surfaces through the adjacent particles. Such anisotropic electron flow in the superstructure significantly retarded the charge recombination with holes at basal {001} facets, leading to better photocatalytic oxidation of 4-chlorophenol (4-CP) and rhodamine B (RhB) than the disordered systems. With the aim to further support the mechanism of anisotropic electron flow in the superstructures, the selective photochemical deposition of cobalt phosphate (CoPi), which facilitate charge separation and photocatalytic water splitting, was carried out.[47] It was revealed that holes transfer to the Co species (Co^{II} and Co^{III}) and produce the CoPi catalyst on the {001} facets upon UV light irradiation,[48] while electrons preferentially transfer to lateral {101} facets for Pt deposition. The spatial modification of co-catalysts, i.e. CoPi as an efficient oxygen-evolving catalyst[48-49] and Pt nanoparticles for hydrogen evolution,[50] largely inhibites the undesired charge recombination. In this case, active $Co^{III/IV}$ species in CoPi can oxidize probe dyes, 3'-*p*-aminophenyl fluorescein (APF) and 3'-*p*-hydroxyphenyl fluorescein (HPF), to generate fluorescein as a fluorescent product at the basal surface via *O*-dearylation reaction (Figure 8d). It was an interesting finding that spatial charge separation with long-lived component can significantly promote photocatalytic efficiency.

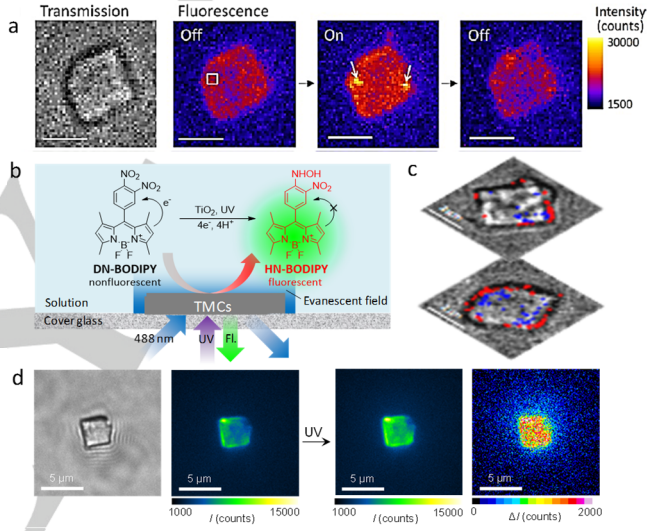

Figure 8. (a) Optical transmission image of 0.04 wt% Au/TMCs and its successive fluorescence images on and off events in Ar-saturated DN-BODIPY solution. The scale bars are 2 μm. (b) Single-molecule fluorescence observation by TIRF microscopy. (c) Transmission images of TMCs (top) and 0.04 wt% Au/TMCs (bottom). The blue and red dots indicate the location of fluorescence bursts on the basal and lateral surfaces of the crystal, respectively. (d) Optical transmission and fluorescence images of a single CoPi-TMC crystal before and after the UV light irradiation and the subtracted image before the UV light irradiation from the image just after the UV light irradiation. Figure reproduced with permission from refs.[20] and [50b]

3.3. Laser flash photolysis

To evaluate the charge dynamics in photocatalytic reactions, the TDR spectroscopy is a powerful technique.[51] Here, 4-(methylthio)phenyl methanol (MTPM) was selected as the probe molecule to monitor the lifetime of the charge-separated state of TMCs after 355-nm laser excitation.[51] It is clear to see the absorption band of MTPM radical cation ($MTPM^{\bullet+}$) around 550 nm, indicating the one-electron oxidation of MTPM by photogenerated holes in TMCs (Figure 9a). Due to the superstructure-induced charge separation, the half-lives of $MTPM^{\bullet+}$ became much longer (~2 μs) than that of Nano (~0.5 μs) as shown in Figure 9b. That is the main reason why TMCs exhibit superior photocatalytic

efficiency than the disordered systems such as Nano. Further to explore the intrinsic physicochemical properties of mesocrystals, it was meaningful to investigate the charge transfer dynamics after electron injection, especially from plasmonic metals. After the 530-nm laser excitation of the Au/TMCs, a broad absorption band, superimposed with those of the trapped electrons and free electrons (600−1000 nm) from reduced TiO_2, appeared in the whole wavelength region (Figure 9c). From the kinetic parameters of decay curves (Figure 9d), it was revealed that the electrons from the excited Au nanoparticles were injected to the conduction band (CB) of TMC within a subpicosecond time scale. It was noteworthy that the injected electrons are inclined to migrate from the basal surfaces to the edges of TMC due to the crystal-face dependent electron trapping probability,[20] thus inhibiting the charge recombination process between the electrons in TMCs and the holes in Au. For a time period of 1.0−3000 ps, the concentration of the electrons in TMC decreased in a multiexponential fashion due to the charge recombination of such stored electrons with the holes in the Au. Further to resolve this problem, the preferable loading of Pt on lateral surface of Au/TMCs was carried out to largely enhance the visible-light photocatalytic performance for hydrogen evolution. This phenomenon was observed here for the first time and implies a fast charge recombination between the trapped electrons in TiO_2 and the holes in Au prior to diffusion from the vicinity of the Au. This work created new avenues for the design of efficient plasmonic photocatalysts with potential applications in solar energy conversion.[43e, 52]

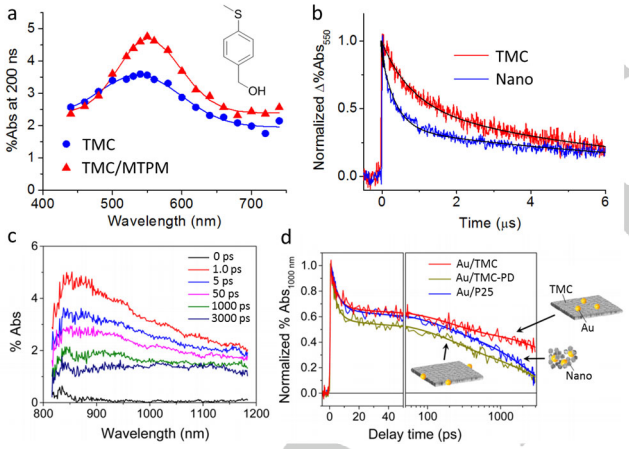

Figure 9. (a) TDR spectra observed at 200 ns after 355-nm laser flash photolysis of TMC in the absence and presence of MTPM. (b) Differential time traces at 550 nm (assigned to $MTPM^{\bullet+}$) for TMC and Nano. (c) TDR spectra observed after 530-nm laser flash photolysis of Au/TMC in ambient air. (d) Normalized transient absorption traces observed at 1000 nm for Au/TMC, Au/TMC-PD (photodeposition), and Au/P25. Figure reproduced with permission from refs.[9e] and [43b]

4. The application of mesocrystals

Over years, mesocrystals worked as biological and bio-inspired mesoscale structures consisting of oriented nanocrystalline units.[53] Mesoporous semiconductors with higher conductivity and electron mobility will provide a series of application of energy harvesting and conversion among solar fuel, photocatalysis, and electrical energy storage technologies.[6] In a wide range of mesocrystals, i.e. $CaCO_3$, $BaSO_4$, metal oxides, metal tungstates and chromates, NH_4TiOF_3, $(NH_4)_3PW_{12}O_{40}$, $LiFePO_4$, metal chalcogenides, noble metals, and organic materials, series of materials with unique properties have been successfully developed.[6, 54] With controllable formation of TMCs through topotactic transformation,[15e, 15f] hydrothermal/solvothermal method,[15b, 15d, 17a, 17c, 17d, 18-19] and growth on supports,[55] there is particular attention paid to potential applications in lithium ion batteries, photocatalysis, enzyme immobilization,[15d] and antireflection materials.[9d]

4.1. Lithium storage

In the past decade, lithium demand has rapidly increased as an efficient energy storage system to lead the market, even though other innovative exploitations of sodium resources and polymeric electrolytes have developed for reliable cost-saving, environment-friendly, and good battery safety.[56] As alternative electrode materials for lithium ion batteries, there is much interest in mesocrystals (e.g., TiO_2,[15b, 17c, 19a] Co_3O_4,[40c] WO_3,[41a] and Fe_2O_3[38b, 38c]), that represent the intricate relationship between superstructure and function.[56f] Compared with nanocrystals as an anode material, the anatase TMC with spindle-shape showed improved lithium insertion behavior (Figure 10a, inset).[19a] It found the nanoporous TMC with well connection of crystallographically oriented nanocrystals has few grain boundaries than disordered nanocrystals system with irregularly oriented connection. The rate capability of the anatase TMCs and the nanocrystals (~15 nm in size) was found from 0.05 to 2 C (1 C = 170 mAh g^{-1}) for five cycles at each current rate (Figure 10a). In addition, the TMCs could deliver specific discharge capacities of 164.9 and 151.7 mA•h g^{-1} at 1 and 2 C, respectively. Between the TMC-based electrode and electrolyte, TMCs provided the properties of facile electronic conduction and fast Li ion transport, which are attributed to the intrinsic characteristics of the mesocrystals with large specific surface area and uniform nanopores. After 60 cycles (Figure 10b), the TMC still maintained good discharge capacity around 74.2% (151.9 mA•h g^{-1}) of the initial one (204.7 mA•h g^{-1}). Similarly, the TMC in rutile phase exhibited the large reversible charge–discharge capacity and excellent cycling performance in lithium-ion batteries.[15b, 17c] In addition, the mesocrystals showed a better performance than their related counterparts.[56g] From the considerable study, the use of mesocrystals is feasible for the promising candidate of the anode or cathode material in lithium ion batteries.[56f]

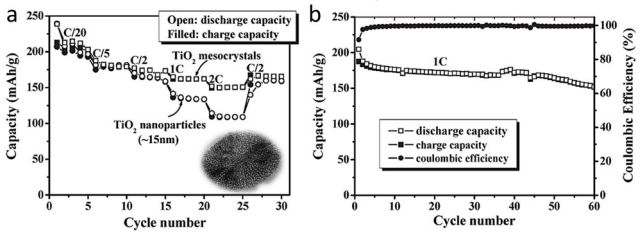

Figure 10. (a) The rate capability of mesocrystals and nanocrystals of anatase TiO_2 from C/20 to 2C (1C = 170 mA•g^{-1}) for five cycles and (b) comparison of cycling performance between them with current rate of 1C. The inset in (a) shows the TEM image of TiO_2 mesocrystal. Figure reproduced with permission from ref.[19a]

4.2. Photocatalysis

Semiconductor-based photocatalysts have gained increasing interest in the harvesting of solar energy for conversion into chemical energy. Because of the nature and structural characteristics of the materials, the promising capabilities are considerred as the essential points for artifical photocatalysis.[5,43] Similar to the electrode materials, mesocrystals with high porosity are considered as efficient photocatalytic materials. The superior performance of various mesocrystals is mainly due to the high porosity, good crystallinity, and even proper exposed facets. The mesocrystals have better potential efficiency than bulk single crystals and disordered nanoparticles. To this point, it was revealed that TMCs enhance the photocatalytic properties in the pollutant dye decomposition[15d] and photocatalytic hydrogen evolution reaction (HER).[57] The mesocrystals typically expose specific crystal facets on the surface. The plate-like TMCs exhibited good performance for the photocatalytic oxidation of 4-chlorophenol and rhodamine B as well as for the photocatalytic reduction of Cr^{6+} in water.[9e] It exhibited a 100–300% photocatalytic enhancement relative to that of anatase Nano with dominant {001} facets and nearly similar to that of benchmark Degussa P25 TiO_2. The enhanced efficiency of photocatalytic reactions was consistent with their charge transfer dynamics in TDR. Further development of the TMCs with tunable facet is interesting to understand the structural morphology (TMC-1–4 with different {001}/{101} ratios) related to fundamental redox catalysis.[44a] It means that the proportion of {001} surfaces increased and that of {101} surfaces decreased due to the oriented crystal growth along the [101] axis (Figure 11c). The degradation efficiency of 4-chlorophenol (4-CP) under UV light irradiation clearly increased in proportion to the amount of {001} surfaces (Figure 11a, red column) attributed to their strong ability to form hydroxyl radicals in this facet.[58] When compared to oxidative degradation, the photocatalytic reduction of Cr^{6+} increased in the order of TMC-4 < TMC-3 < TMC-2 < TMC-1 (Figure 11a, green column), as well as the photocatalytic HER (Figure 11a, blue column). It was obvious that eosin Y dye (EY)-sensitized HER on Pt/TMC increased as {001}/{101} decreased (Figure 11b, pink column).[59] In the EY-sensitized system (Figure 11c, purple part), the electrons are delivered by freely diffusing $EY^{\bullet 3-}$, which is generated by electron-transfer reactions between $^{1,3}(EY^{2-})^*$ and triethanolamine (TEOA). The injected electrons then transfer to Pt nanoparticles deposited on the TMC {101} facets to produce poor H_2 due to low concentrations of adsorbed EY. In contrast, Ruthenizer 470 is more efficiently adsorbed on the {001} facets, inducing higher HER related to higher values of {001}/{101} (Figure 11b, light blue column). The electrons directly injected from the excited Ru can avoid charge recombination with the dye cations remaining on the {001} surface, because the electrons efficiently migrate across the assembled nanocrystals interface and reach the Pt co-catalyst on the {101} surface (Figure 11c, red part). Interestingly, the reaction preference can be found for several TMCs with dominant facets,[9f, 15b] as well as the excellent HER with Pt or mental-free modification.[43b, 43f, 44a] The preferable crystal-facet-dependent surface adsorption and charge transfer hold great promise for improving the photocatalytic performance than conventional disordered systems (Nano) in pollutant degradation and HER. In addition to anatase TMCs, rutile phase and several other mesocrystals were synthesized and exhibited excellent photocatalytic ability.[6d, 56g] In particular, it is of great interest to develop Ti-based ternary perovskite oxides with mesocrystal superstructures for revealing the superstructure-dependent activity in solar energy conversion. Very recently, a novel perovskite $SrTiO_3$ mesocrystal (SMC) with well-defined orientation of assembled cubic nanocrystals was synthesized by topotactic epitaxy from TMC.[29b] Compared to the disordered system (Nano), the SMC-48 (hydrothermal treatment time, 48 h) with efficient interparticle charge transfer along the ordered internal nanocubes to the termination at the larger active external cubes (Figure 11d) exhibited remarkably long-lived charges for high quantum yield and good durability in overall water splitting (Figure 11e). Such perovskite-type mesocrystals with mechanistic insight into the heterogeneous charge transfer will provide new strategies for the fields of photocatalysis and optoelectronics.

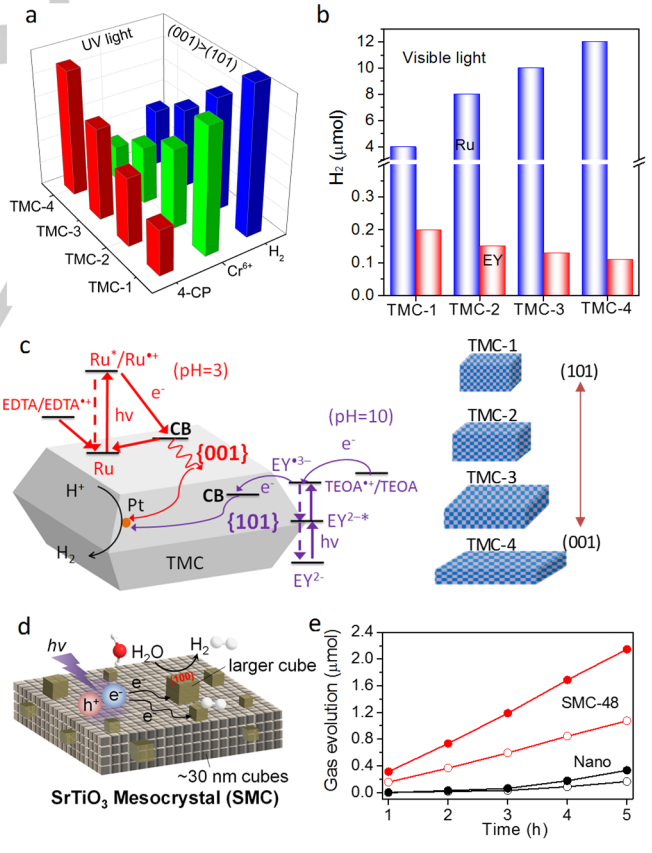

Figure 11. (a) Comparison of photocatalytic degradation of 4-chlorophenol (4-CP), Cr^{6+} and HER in UV light excitation, and (b) dye-sensitized HER under visible light irradiation. (c) Schematic illustration of charge transfer from Pt/TMC in aqueous solution (pH 10) containing Eosin Y (EY) and TEOA, and in aqueous

solution (pH 3) containing Ruthenizer 470 (Ru) and EDTA. The inset in (c) shows the synthesis of different-shaped TMCs related to the {101}/{001}. (d) Anisotropic electron transport from the innner nanocubes to the outer ones on SMC and (e) the comparison of H_2 (solid circles) and O_2 (open circles) evolution between SMC and Nano under UV light irradiation. Figure reproduced with permission from ref.[44a] and [29b]

4.3. Gas sensor

For rapid detection and quantification of gas species in combustion environment, it is an urgent requirement to develop the nanomaterial-based sensing technologies through the energy harvesting from thermal radiation, incident light, and piezoelectricity.[61-64] In this case, the unique porous frameworks with single crystal feature are considered as effective adsorbents for pollutant dye and functional molecule, especially for TMC than commercial TiO_2 (P25).[9g, 18, 60] It should be noted that the mesocrystal would be of great interest to be developed as gas sensor because of their high porosity and specific surface as well as the ordered mesocrystalline structure. Except for the NO removal,[17b] the $W_{18}O_{49}$ mesocrystals with more oxygen vacancies exhibited higher response (1 ppm) and sensing response (50 ppb) for NO_2 than that of nanowires.[41b] After that, reduced graphene oxide (rGO)-conjugated Cu_2O nanowire mesocrystals achieved better sensitivity for NO_2 at room temperature, when compared to Cu_2O nanowire networks and rGO sheets.[61] Another CuO mesocrystal from pulse laser treatment also exhibited the higher sensitivity and better selectivity towards ethanol.[62] Meanwhile, it was found that the ZnO-CuO mesocrystal composite or Au nanostar-encrusted ZnO mesocrystals showed good selectivity towards H_2S gas.[63] In addition, the SnO_2 mesocrystal with mixed phase exhibited superior discrimination of ethanol from acetone, methanol, and benzene than that of the SnO_2 with a single phase or a solid structure.[64] As one of most important p-type oxide semiconductors, Co_3O_4 mesocrystals synthesized through the polymer mediated route displayed superior gas-sensing properties on formaldehyde and ethanol.[40a] Figure 12a shows the representative dynamic gas response of the Co_3O_4 materials to formaldehyde and ethanol with concentrations ranging from 5 ppm to 1000 ppm. The sensing responses of the Co_3O_4 mesocrystal sensor to 100 ppm of formaldehyde and ethanol were around 2.8 and 1.5, in contrast to 1.5 and 1.1 with the Co_3O_4 powder, respectively. It was found that the sensing responses of Co_3O_4 mesocrystals firstly increased with its vapour concentrations rapidly below 100 ppm and slowly tend to subsequent saturation, while Co_3O_4 powder displayed poor sensing responses (Figure 12b). The unique mesocrystal structure with voids between primary nanocrystals could induce the convenient gas diffusion and mass transportation and provide more active sites for gas sensing.[40a]

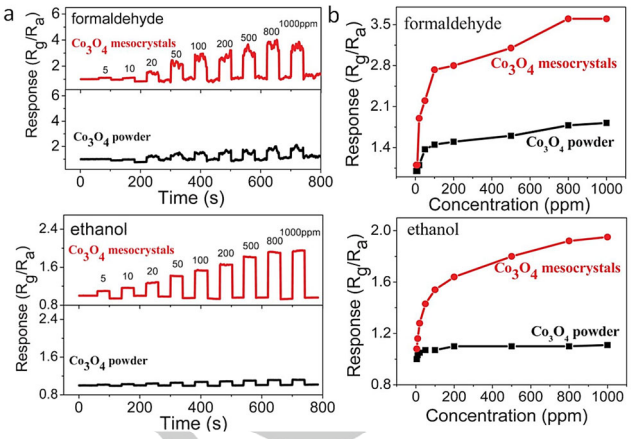

Figure 12. (a) The response-recovery curves and (b) gas concentration-dependent responses of the two sensors based on the Co_3O_4 mesocrystals and Co_3O_4 powder to formaldehyde and ethanol, respectively. The R_a is the sensor resistance in air and R_g is the sensor resistance in test gas. Figure reproduced with permission from ref.[40a]

4.4. Biomedical materials

Among the conversion from magnetic energy to kinetic and thermal energies, nanostructured magnetic materials with drug molecules have attracted increasing attention because of the emerging applications of drug release and hyperthermia with combined chemotherapy in biomedical treatment.[65,67] Due to their good biocompatibility, mesocrystals have been tentatively examined as biomedical materials in drug delivery and magnetic resonance imaging.[65] In this case, superparamagnetic $CaCO_3$ mesocrystals was developed to deliver Au–DNA nanoparticles and DOX (doxorubicin) as a MDS (multistage delivery system) for cancer therapy.[66] The mesocrystalline $CaCO_3$ particles with high porosity can encapsulate DOX, Au–DNA, and Fe_3O_4@silica nanoparticles for magnetic control and therapy. As stage 1 microparticles (S1MPs), the nanoparticles–$CaCO_3$ system (NCS) was used to protect functional sections from degradation and phagocytosis in blood circulation. When the particle margination in vascular walls, the Au–DNA nanoparticles (stage 2 nanoparticles, S2NPs) and DOX were gradually released from S1MPs by degradation towards targeted tissues for biomedical therapy. The NCS exhibits good intracellular delivery, especially in nuclear invasion, and was thus proposed as a potential co-delivery system for drug and gene therapy among gene and intracellular transport of DOX in vitro. The co-delivery of DOX and Au–DNA nanoparticles by the $CaCO_3$ mesocrystals was verified on HeLa cells and A549 cells. The empty $CaCO_3$ mesocrystals were biocompatible as suggested by the low cytotoxicity (Figure 13a). Subsequently, DOX and DNA were successfully delivered into the right intracellular locations in the cell (Figure 13b-f).[56g] Finally, gene therapy can be achieved by incorporating Au nanoparticles through the plasmid of enhanced green fluorescent protein (pDNA). This platform exhibited an efficient approach in the targeted delivery of therapeutic nanoparticles and molecules via a multistage strategy and was considered as a potential

system in co-delivery of multiple agents for biomedical imaging and therapy.[67]

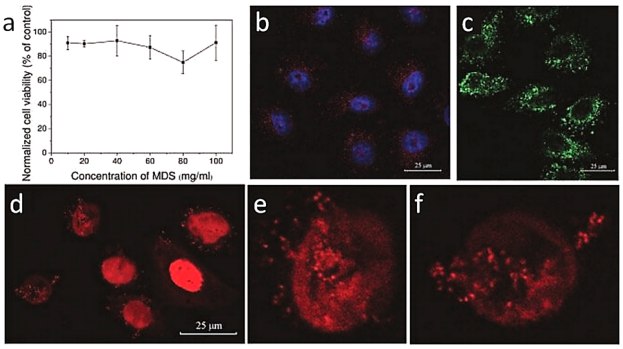

Figure 13. Cytotoxicity of the MDS (without DOX and pDNA) on HeLa cells for 12 h, ATTC CCL2. (b-e) Confocal laser scanning microscopy images for in vitro evaluation of the MDS containing DOX and pDNA on HeLa cells. (b) Cellular uptake of the MDS (with Au–DNA nanoparticles) for 4 h; merged image: cell nuclei were dyed blue by Hoechst 33258 and pDNA residues were dyed red by EtBr. (c) HeLa cells were transfected by the MDS (with Au–DNA nanoparticles). Green fluorescent proteins (green) only exist in the cells successfully transfected by pEGFP. (d) Cellular uptake of the MDS (with DOX) for 4 h; DOX shows as red dots. (e, f) Enlarged images of (d). Figure reproduced with permission from ref.[66]

5. Conclusions and outlook

Mesocrystals are of considerable interest in the fields of nanoscience and nanotechnology as well as biominerals over the past decades. The proposed growth followed the procedures of phase separation, matrix-mediated mesophase transformation, and self-assembly of the mesoscale building blocks.[6a, 6b] In this review, we firstly summarized the recent synthesis of various mesocrystals via the versatile topotactic transformation. Following this strategy, it is prominent to provide the opportunities and challenges for designing and fabricating attractive hierarchical superstructures and other epitaxial or composited mesocrystals. On the other hand, underlying mechanisms related to formation processes remain unresolved. To this point, intensive efforts have been made from real-time video microscopy to provide real-time information about crystallization, which is strongly related to the structure-property relationships.[68] From the mechanistic insight into particle-mediated growth, it would be highly desirable tailoring the crystallographical alignment into new mesocrystals with unique functions, or directly fabricate hierarchical assemblies of dimensional architectures.[69]

Understanding and exploring their functions of mesocrystals are continuing challenges in promoting the reaction efficiency.[70] According to the recent investigations on spatial and temporal scales, mesocrystals, mostly TMCs, possess intrinsic performance in charge separation. The dramatic enhancement in a wide range of applications derives from their high specific surface area and ordered mesoporous structures. That is (i) the high specific surface area that provides abundant adsorption sites for reactants; (ii) the porous structure that allows efficient mass transport of reactants and products; (iii) the oriented arrangement that mediates anisotropic carrier flow to suppress the recombination of electron–hole pairs. Not only the studies in ensemble-averaged measurements, but further major challenges to explore the complexity and inhomogeneity of the reaction dynamics in mesocrystal will call for both higher and super spatial and temporal resolutions at ultimate techniques, i.e. the combination of single-molecule (or single-particle) time-resolved spectroscopy, femtosecond ultrafast spectroscopy, and even electrochemical AFM.

Further explorations of the mesocrystals and their related structures exhibited the key advance in a wide filed of energy harvesting, storage, conversion, and environmental remediation as well.[71] To promote the reaction efficiency, numerous strategies are of considerable interest in band engineering, morphology tailoring, co-catalysts assistance, cooperative reorganization and even reaction environment optimization. It is noteworthy that design and synthesis of superstructures are still one of the key and prominent topics in current research and application ranging from UV to visible light due to their efficient charge separation. In particular, the mesocrystals provide a promising way toward novel nanofabrication technique for making functional porous architectures and electronic devices. A stimulus for design of superstructures with mutual orientation will open a new avenue for crystal engineering in environment remediation and solar energy conversion.

Acknowledgements

This work has been partly supported by PRESTO, JST, and a Grant-in-Aid for Scientific Research (Project 25220806, 25288035, and others) from the Ministry of Education, Culture, Sports, Science and Technology (MEXT) of the Japanese Government.

Keywords: Mesocrystal • Crystal growth • Topotactic transformation • Anisotropic charge separation • Charge transfer dynamics

[1] a) C. Perego, R. Millini, *Chem. Soc. Rev.,* **2013**, *42*, 3956-3976; b) E. J. W. Crossland, N. Noel, V. Sivaram, T. Leijtens, J. A. Alexander-Webber, H. J. Snaith, *Nature* **2013**, *495*, 215-219; c) M. M. Lee, J. Teuscher, T. Miyasaka, T. N. Murakami, H. J. Snaith, *Science* **2012**, *338*, 643-647; d) T. Wagner, S. Haffer, C. Weinberger, D. Klaus, M. Tiemann, *Chem. Soc. Rev.,* **2013**, *42*, 4036-4053; e) A. Walcarius, *Chem. Soc. Rev.,* **2013**, *42*, 4098-4140; f) Y. Ye, C. Jo, I. Jeong, J. Lee, *Nanoscale* **2013**, *5*, 4584-4605.

[2] M. E. Davis, *Nature* **2002**, *417*, 813-821.

[3] W. Li, J. Liu, D. Zhao, *Nat. Rev. Mater.,* **2016**, *1*, 16023.

[4] D. Li, H. Zhou, I. Honma, *Nat. Mater.,* **2004**, *3*, 65-72.

[5] a) Y. Park, W. Kim, D. Monllor-Satoca, T. Tachikawa, T. Majima, W. Choi, *J. Phys. Chem. Lett.,* **2013**, *4*, 189-194; b) M. Kong, Y. Li, X. Chen, T. Tian, P. Fang, F. Zheng, X. Zhao, *J. Am. Chem. Soc.,* **2011**, *133*, 16414-16417; c) N. Lakshminarasimhan, E. Bae, W. Choi, *J. Phys. Chem. C* **2007**, *111*, 15244-15250; d) N. Lakshminarasimhan, W. Kim, W. Choi, *J. Phys. Chem. C* **2008**, *112*, 20451-20457; e) S. K. Choi, S. Kim, S. K. Lim, H. Park, *J. Phys. Chem. C* **2010**, *114*, 16475-16480; f) A. A. Ismail, D. W. Bahnemann, *J. Phys. Chem. C* **2011**, *115*, 5784-5791; g) S. Tirosh, T. Dittrich, A. Ofir, L. Grinis, A. Zaban, *J. Phys. Chem. B* **2006**, *110*,

16165-16168; h) J. P. Gonzalez-Vazquez, V. Morales-Flórez, J. A. Anta, *J. Phys. Chem. Lett.,* **2012**, *3*, 386-393.

[6] a) L. Zhou, P. O'Brien, *Small* **2008**, *4*, 1566-1574; b) R. Q. Song, H. Colfen, *Adv. Mater.,* **2010**, *22*, 1301-1330; c) J. X. Fang, B. J. Ding, H. Gleiter, *Chem. Soc. Rev.,* **2011**, *40*, 5347-5360; d) L. Zhou, P. O'Brien, *J. Phys. Chem. Lett.,* **2012**, *3*, 620-628.

[7] a) H. Cölfen, M. Antonietti, *Mesocrystals and Nonclassical Crystallization*, Wiley, **2008**; b) H. Cölfen, M. Antonietti, *Angew. Chem., Int. Ed.,* **2005**, *44*, 5576-5591; c) M. Niederberger, H. Cölfen, *Phys. Chem. Chem. Phys,* **2006**, *8*, 3271-3287.

[8] J. Seto, Y. R. Ma, S. A. Davis, F. Meldrum, A. Gourrier, Y. Y. Kim, U. Schilde, M. Sztucki, M. Burghammer, S. Maltsev, C. Jager, H. Colfen, *Proc. Natl. Acad. Sci. U. S. A.,* **2012**, *109*, 7126-7126.

[9] a) L. Zhou, D. Smyth-Boyle, P. O'Brien, *J. Am. Chem. Soc.,* **2008**, *130*, 1309-1320; b) Z. Bian, J. Zhu, J. Wen, F. Cao, Y. Huo, X. Qian, Y. Cao, M. Shen, H. Li, Y. Lu, *Angew. Chem., Int. Ed.,* **2011**, *50*, 1105-1108; c) H. Yu, B. Tian, J. Zhang, *Chem. Eur. J,* **2011**, *17*, 5499-5502; d) J. Cai, J. Ye, S. Chen, X. Zhao, D. Zhang, S. Chen, Y. Ma, S. Jin, L. Qi, *Energy Environ. Sci.,* **2012**, *5*, 7575-7581; e) Z. Bian, T. Tachikawa, T. Majima, *J. Phys. Chem. Lett.,* **2012**, *3*, 1422-1427; f) Q. Chen, W. Ma, C. Chen, H. Ji, J. Zhao, *Chem. Eur. J,* **2012**, *18*, 12584-12589; g) L. Zhou, J. Chen, C. Ji, L. Zhou, P. O'Brien, *CrystEngComm* **2013**, *15*, 5012-5015; h) Z. Li, A. Gessner, J.-P. Richters, J. Kalden, T. Voss, C. Kuebel, A. Taubert, *Adv. Mater.* **2008**, *20*, 1279-1285; i) Z. Liu, X. D. Wen, X. L. Wu, Y. J. Gao, H. T. Chen, J. Zhu, P. K. Chu, *J. Am. Chem. Soc.,* **2009**, *131*, 9405-9412; jX. L. Wu, S. J. Xiong, Z. Liu, J. Chen, J. C. Shen, T. H. Li, P. H. Wu, P. K. Chu, *Nat. Nanotechnol.* **2011**, *6*, 103-106; k) M. Distaso, R. N. Klupp Taylor, N. Taccardi, P. Wasserscheid, W. Peukert, *Chem. Eur. J,* **2011**, *17*, 2923-2930; lM. Distaso, D. Segets, R. Wernet, R. K. Taylor, W. Peukert, *Nanoscale* **2012**, *4*, 864-873; m) E. Hosono, T. Tokunaga, S. Ueno, Y. Oaki, H. Imai, H. Zhou, S. Fujihara, *Cryst. Growth Des.,* **2012**, *12*, 2923-2931; n) M.-H. Liu, Y.-H. Tseng, H. F. Greer, W. Zhou, C.-Y. Mou, *Chem. Eur. J,* **2012**, *18*, 16104-16113; o) S. Sun, X. Zhang, J. Zhang, X. Song, Z. Yang, *Cryst. Growth Des.,* **2012**, *12*, 2411-2418; p) F. Waltz, G. Wissmann, J. Lippke, A. M. Schneider, H.-C. Schwarz, A. Feldhoff, S. Eiden, P. Behrens, *Cryst. Growth Des.,* **2012**, *12*, 3066-3075; q) H. Wang, L. Xin, H. Wang, X. Yu, Y. Liu, X. Zhou, B. Li, *RSC Adv.,* **2013**, *3*, 6538-6544; r) S.-S. Wang, A.-W. Xu, *CrystEngComm* **2013**, *15*, 376-381; s) G.-S. Park, D. Shindo, Y. Waseda, T. Sugimoto, *J. Colloid Interface Sci.,* **1996**, *177*, 198-207; t) X.-L. Fang, C. Chen, M.-S. Jin, Q. Kuang, Z.-X. Xie, S.-Y. Xie, R.-B. Huang, L.-S. Zheng, *J. Mater. Chem.,* **2009**, *19*, 6154-6160; u) J. S. Chen, T. Zhu, C. M. Li, X. W. Lou, *Angew. Chem., Int. Ed.,* **2011**, *50*, 650-653; v) J. Ma, J. Teo, L. Mei, Z. Zhong, Q. Li, T. Wang, X. Duan, J. Lian, W. Zheng, *J. Mater. Chem.,* **2012**, *22*, 11694-11700; w) T. He, D. Chen, X. Jiao, *Chem. Mater.,* **2004**, *16*, 737-743; xH. G. Yang, H. C. Zeng, *Angew. Chem., Int. Ed.,* **2004**, *43*, 5930-5933; y) Z. Zhuang, F. Huang, Z. Lin, H. Zhang, *J. Am. Chem. Soc.,* **2012**, *134*, 16228-16234; z) J. Zhao, R. Tan, Y. Guo, Y. Lu, W. Xu, W. Song, *CrystEngComm* **2012**, *14*, 4575-4577; aa) J. Fang, P. M. Leufke, R. Kruk, D. Wang, T. Scherer, H. Hahn, *Nano Today* **2010**, *5*, 175-182; ab) B. Liu, H. C. Zeng, *J. Am. Chem. Soc.,* **2004**, *126*, 8124-8125; ac) W.-T. Yao, S.-H. Yu, Y. Zhou, J. Jiang, Q.-S. Wu, L. Zhang, J. Jiang, *J J. Phys. Chem. B* **2005**, *109*, 14011-14016; ad) M. Xu, F. Wang, B. Ding, X. Song, J. Fang, *RSC Adv.,* **2012**, *2*, 2240-2243.

[10] a) F. Huang, H. Zhang, J. F. Banfield, *Nano Lett.,* **2003**, *3*, 373-378; b) J. H. Yu, J. Joo, H. M. Park, S.-I. Baik, Y. W. Kim, S. C. Kim, T. Hyeon, *J. Am. Chem. Soc.,* **2005**, *127*, 5662-5670; c) A. Querejeta-Fernandez, J. C. Hernandez-Garrido, H. Yang, Y. Zhou, A. Varela, M. Parras, J. J. Calvino-Gamez, J. M. Gonzalez-Calbet, P. F. Green, N. A. Kotov, *ACS Nano* **2012**, *6*, 3800-3812; d) K.-S. Cho, D. V. Talapin, W. Gaschler, C. B. Murray, *J. Am. Chem. Soc.,* **2005**, *127*, 7140-7147; e) Y. Nagaoka, O. Chen, Z. Wang, Y. C. Cao, *J. Am. Chem. Soc.,* **2012**, *134*, 2868-2871; fQ. Chen, C. Jia, Y. Li, J. Xu, B. Guan, M. Z. Yates, *Langmuir* **2017**, *33*, 2362-2369; g) P. Simon, E. Rosseeva, I. A. Baburin, L. Liebscher, S. G. Hickey, R. Cardoso-Gil, A. Eychmüller, R. Kniep, W. Carrillo-Cabrera, *Angew. Chem., Int. Ed.,* **2012**, *124*, 10934-10939.

[11] a) J. Fang, X. Ma, H. Cai, X. Song, B. Ding, *Nanotechnology* **2006**, *17*, 5841-5845; b) M. Giersig, I. Pastoriza-Santos, L. M. Liz-Marzán, *J. Mater. Chem.,* **2004**, *14*, 607-610; c) J. Fang, B. Ding, X. Song, *Appl. Phys. Lett.,* **2007**, *91*, 083108/083101-083108/083103; d) Y. Cao, J. Fan, L. Bai, P. Hu, G. Yang, F. Yuan, Y. Chen, *CrystEngComm* **2010**, *12*, 3894-3899; e) Y. Yamauchi, T. Momma, M. Fuziwara, S. S. Nair, T. Ohsuna, O. Terasaki, T. Osaka, K. Kuroda, *Chem. Mater.,* **2005**, *17*, 6342-6348; f) T. Li, H. You, M. Xu, X. Song, J. Fang, *ACS Appl. Mater. Inter.,* **2012**, *4*, 6942-6948; g) X. Huang, S. Tang, J. Yang, Y. Tan, N. Zheng, *J. Am. Chem. Soc.,* **2011**, *133*, 15946-15949.

[12] a) S. Wohlrab, N. Pinna, M. Antonietti, H. Cölfen, *Chem. Eur. J,* **2005**, *11*, 2903-2913; b) D. D. Medina, Y. Mastai, *Cryst. Growth Des.,* **2008**, *8*, 3646-3651; cY. Jiang, H. Gong, D. Volkmer, L. Gower, H. Cölfen, *Adv. Mater.* **2011**, *23*, 3548-3552; dM. Huang, U. Schilde, M. Kumke, M. Antonietti, H. Cölfen, *J. Am. Chem. Soc.,* **2010**, *132*, 3700-3707.

[13] H. Li, M. Guan, G. Zhu, G. Yin, Z. Xu, *Cryst. Growth Des.,* **2016**, *16*, 1306-1310.

[14] A. Fujishima, K. Honda, *Nature* **1972**, *238*, 37-38.

[15] a) F. F. Chen, F. L. Cao, H. X. Li, Z. F. Bian, *Langmuir* **2015**, *31*, 3494-3499; b) Z. S. Hong, M. D. Wei, T. B. Lan, L. L. Jiang, G. Z. Cao, *Energy Environ. Sci.,* **2012**, *5*, 5408-5413; c) W. Jiao, L. Z. Wang, G. Liu, G. Q. Lu, H. M. Cheng, *ACS Cata.,* **2012**, *2*, 1854-1859; d) P. Tartaj, *Chem. Commun.,* **2011**, *47*, 256-258; e) Y. Q. Liu, Y. Zhang, H. Tan, J. Wang, *Cryst. Growth Des.,* **2011**, *11*, 2905-2912; f) J. Y. Feng, M. C. Yin, Z. Q. Wang, S. C. Yan, L. J. Wan, Z. S. Li, Z. G. Zou, *CrystEngComm* **2010**, *12*, 3425-3429.

[16] C. W. Abney, K. M. L. Taylor-Pashow, S. R. Russell, Y. Chen, R. Samantaray, J. V. Lockard, W. B. Lin, *Chem. Mater.,* **2014**, *26*, 5231-5243.

[17] a) S. J. Liu, J. Y. Gong, B. Hu, S. H. Yu, *Cryst. Growth Des.,* **2009**, *9*, 203-209; b) D. Q. Zhang, G. S. Li, F. Wang, J. C. Yu, *CrystEngComm* **2010**, *12*, 1759-1763; c) Z. Hong, M. Wei, T. Lan, G. Cao, *Nano Energy* **2012**, *1*, 466-471; d) H. Wang, Y. Liu, Z. Liu, H. M. Xu, Y. J. Deng, H. Shen, *CrystEngComm* **2012**, *14*, 2278-2282.

[18] L. Li, C. Y. Liu, *CrystEngComm* **2010**, *12*, 2073-2078.

[19] a) J. F. Ye, W. Liu, J. G. Cai, S. A. Chen, X. W. Zhao, H. H. Zhou, L. M. Qi, *J. Am. Chem. Soc.,* **2011**, *133*, 933-940; b) R. O. Da Silva, R. H. Goncalves, D. G. Stroppa, A. J. Ramirez, E. R. Leite, *Nanoscale* **2011**, *3*, 1910-1916; c) P. Tartaj, J. M. Amarilla, *Adv. Mater.,* **2011**, *23*, 4904-4907.

[20] Z. Bian, T. Tachikawa, W. Kim, W. Choi, T. Majima, *J. Phys. Chem. C* **2012**, *116*, 25444-25453.

[21] a) X. Ge, C. D. Gu, X. L. Wang, J. P. Tu, *J. Colloid Interface Sci.,* **2015**, *438*, 149-158; b) J. B. Fei, Y. Cui, X. H. Yan, W. Qi, Y. Yang, K. W. Wang, Q. He, J. B. Li, *Adv. Mater.,* **2008**, *20*, 452-456; c) W. Xiao, D. Wang, X. W. Lou, *J. Phys. Chem. C* **2010**, *114*, 1694-1700; d) J. Liu, J. Jiang, M. Bosman, H. J. Fan, *J. Mater. Chem.,* **2012**, *22*, 2419-2426; e) H. B. Wu, J. S. Chen, H. H. Hng, X. Wen Lou, *Nanoscale* **2012**, *4*, 2526-2542.

[22] M. Zheng, H. Dong, Y. Xiao, H. Hu, C. He, Y. Liang, B. Lei, L. Sun, Y. Liu, *J. Mater. Chem. A* **2017**, *5*, 6921-6927.

[23] Z. F. Bian, T. Tachikawa, P. Zhang, M. Fujitsuka, T. Majima, *Nat. Commun.,* **2014**, *5.*

[24] J.-C. Yang, H.-J. Liu, Y.-H. Chu, *MRS Commun.,* **2016**, *6*, 167-181.

[25] a) S. Tominaka, H. Hamoudi, T. Suga, T. D. Bennett, A. B. Cairns, A. K. Cheetham, *Chem. Sci.,* **2015**, *6*, 1465-1473; b) J. Wang, C. F. Tan, T. Zhu, G. W. Ho, *Angew. Chem., Int. Ed.,* **2016**, *55*, 10326-10330; c) S. J. Yang, S. Nam, T. Kim, J. H. Im, H. Jung, J. H. Kang, S. Wi, B. Park, C. R. Park, *J. Am. Chem. Soc.,* **2013**, *135*, 7394-7397.

[26] X. Li, Z. Ao, J. Liu, H. Sun, A. I. Rykov, J. Wang, *ACS Nano* **2016**, *10*, 11532-11540.

[27] a) A. P. Côté, A. I. Benin, N. W. Ockwig, M. O'Keeffe, A. J. Matzger, O. M. Yaghi, *Science* **2005**, *310*, 1166-1170; b) E. Jahnke, I. Lieberwirth, N. Severin, J. P. Rabe, H. Frauenrath, *Angew. Chem., Int. Ed.,* **2006**, *45*,

5383-5386; c) J. W. Lauher, F. W. Fowler, N. S. Goroff, *Acc. Chem. Res.,* **2008**, *41*, 1215-1229; d) A. Matsumoto, K. Sada, K. Tashiro, M. Miyata, T. Tsubouchi, T. Tanaka, T. Odani, S. Nagahama, T. Tanaka, K. Inoue, S. Saragai, S. Nakamoto, *Angew. Chem., Int. Ed.,* **2002**, *41*, 2502-2505; e) A. Matsumoto, T. Tanaka, T. Tsubouchi, K. Tashiro, S. Saragai, S. Nakamoto, *J. Am. Chem. Soc.,* **2002**, *124*, 8891-8902; f) A. Matsumoto, T. Chiba, K. Oka, *Macromolecules* **2003**, *36*, 2573-2575.

[28] a) C. F. Guo, J. M. Zhang, Y. Tian, Q. Liu, *ACS Nano* **2012**, *6*, 8746-8752; b) L. S. Li, N. J. Sun, Y. Y. Huang, Y. Qin, N. Zhao, J. N. Gao, M. X. Li, H. H. Zhou, L. M. Qi, *Adv. Funct. Mater.,* **2008**, *18*, 1194-1201; c) C. F. Guo, S. H. Cao, J. M. Zhang, H. Y. Tang, S. M. Guo, Y. Tian, Q. Liu, *J. Am. Chem. Soc.,* **2011**, *133*, 8211-8215.

[29] a) V. Kalyani, B. S. Vasile, A. Ianculescu, M. T. Buscaglia, V. Buscaglia, P. Nanni, *Cryst. Growth Des.,* **2012**, *12*, 4450-4456; b) P. Zhang, T. Ochi, M. Fujitsuka, Y. Kobori, T. Majima, T. Tachikawa, *Angew. Chem., Int. Ed.,* **2017**, *56*, 5299-5303; c) N. Masuda, Y. Kobayashi, O. Hernandez, T. Bataille, S. Paofai, H. Suzuki, C. Ritter, N. Ichijo, Y. Noda, K. Takegoshi, C. Tassel, T. Yamamoto, H. Kageyama, *J. Am. Chem. Soc.,* **2015**, *137*, 15315-15321.

[30] B. B. Bokhonov, *Dalton Trans.,* **2015**, *44*, 176-181.

[31] a) apos, N. R. Amico, G. Cantele, D. Ninno, *Appl. Phys. Lett.* **2012**, *101*, 141606; b) S. A. Chambers, T. Ohsawa, C. M. Wang, I. Lyubinetsky, J. E. Jaffe, *Surf. Sci.* **2009**, *603*, 771-780; c) A. Lotnyk, S. Senz, D. Hesse, *Thin Solid Films* **2007**, *515*, 3439-3447.

[32] a) M. Huijben, A. Brinkman, G. Koster, G. Rijnders, H. Hilgenkamp, D. H. A. Blank, *Adv. Mater.* **2009**, *21*, 1665-1677; b) L. Li, C. Richter, J. Mannhart, R. C. Ashoori, *Nat. Phys.,* **2011**, *7*, 762-766; c) J. A. Bert, B. Kalisky, C. Bell, M. Kim, Y. Hikita, H. Y. Hwang, K. A. Moler, *Nat. Phys.,* **2011**, *7*, 767-771.

[33] a) F. T. Wagner, G. A. Somorjai, *Nature* **1980**, *285*, 559-560; b) R. Konta, T. Ishii, H. Kato, A. Kudo, *J. Phys. Chem. B* **2004**, *108*, 8992-8995; c) S. Y. Yang, J. Seidel, S. J. Byrnes, P. Shafer, C. H. Yang, M. D. Rossell, P. Yu, Y. H. Chu, J. F. Scott, J. W. Ager, III, L. W. Martin, R. Ramesh, *Nat. Nanotech.,* **2010**, *5*, 143-147; d) J. M. P. Martirez, S. Kim, E. H. Morales, B. T. Diroll, M. Cargnello, T. R. Gordon, C. B. Murray, D. A. Bonnell, A. M. Rappe, *J. Am. Chem. Soc.* **2015**, *137*, 2939-2947.

[34] F. Qi, K. Koji, Y. Kazumichi, *Chem. Lett.,* **2003**, *32*, 48-49.

[35] L. H. Li, J. X. Deng, J. Chen, X. R. Xing, *Chem. Sci.,* **2016**, *7*, 855-865.

[36] T. Yajima, F. Takeiri, K. Aidzu, H. Akamatsu, K. Fujita, W. Yoshimune, M. Ohkura, S. Lei, V. Gopalan, K. Tanaka, C. M. Brown, M. A. Green, T. Yamamoto, Y. Kobayashi, H. Kageyama, *Nat. Chem.,* **2015**, *7*, 1017-1023.

[37] a) D. Wang, J. Li, X. Cao, G. Pang, S. Feng, *Chem. Commun.,* **2010**, *46*, 7718-7720; b) M. Wang, Y. Zhang, Y. Zhou, F. Yang, E. J. Kim, S. H. Hahn, S. G. Seong, *CrystEngComm* **2013**, *15*, 754-763.

[38] a) A. Ahniyaz, Y. Sakamoto, L. Bergström, *Proc. Natl. Acad. Sci. U. S. A.,* **2007**, *104*, 17570-17574; b) X. C. Duan, L. Mei, J. M. Ma, Q. H. Li, T. H. Wang, W. J. Zheng, *Chem. Commun.,* **2012**, *48*, 12204-12206; c) Z. An, J. Zhang, S. Pan, F. Yu, *J. Phys. Chem. C* **2009**, *113*, 8092-8096.

[39] F. Dang, K. Kato, H. Imai, S. Wada, H. Haneda, M. Kuwabara, *Cryst. Growth Des.,* **2011**, *11*, 4129-4134.

[40] a) Y. Liu, G. Zhu, B. Ge, H. Zhou, A. Yuan, X. Shen, *CrystEngComm* **2012**, *14*, 6264-6270; b) D. Hassen, S. A. El-Safty, K. Tsuchiya, A. Chatterjee, A. Elmarakbi, M. A. Shenashen, M. Sakai, *Sci. Rep.,* **2016**, *6*, 24330; c) D. Su, S. Dou, G. Wang, *Nano Res.,* **2014**, *7*, 794-803.

[41] a) X. Duan, S. Xiao, L. Wang, H. Huang, Y. Liu, Q. Li, T. Wang, *Nanoscale* **2015**, *7*, 2230-2234; b) D. Wang, J. Sun, X. Cao, Y. Zhu, Q. Wang, G. Wang, Y. Han, G. Lu, G. Pang, S. Feng, *J. Mater. Chem. A* **2013**, *1*, 8653-8657.

[42] E. Uchaker, M. Gu, N. Zhou, Y. Li, C. Wang, G. Cao, *Small* **2013**, *9*, 3880-3886.

[43] a) P. Zhang, T. Tachikawa, M. Fujitsuka, T. Majima, *ChemSusChem* **2016**, *9*, 617-623; b) Z. Bian, T. Tachikawa, P. Zhang, M. Fujitsuka, T. Majima, *J. Am. Chem. Soc.,* **2014**, *136*, 458-465; c) P. Zhang, M. Fujitsuka, T. Majima, *Appl. Catal., B,* **2016**, *185*, 181-188; d) O. Elbanna, P. Zhang, M. Fujitsuka, T. Majima, *Appl. Catal., B,* **2016**, *192*, 80-87; e) O. Elbanna, S. Kim, M. Fujitsuka, T. Majima, *Nano Energy* **2017**, *35*, 1-8; f) O. Elbanna, M. Fujitsuka, T. Majima, *ACS Appl. Mater. Interfaces*, **2017**, DOI: 10.1021/acsami.7b08548.

[44] a) P. Zhang, T. Tachikawa, Z. Bian, T. Majima, *Appl. Catal., B,* **2015**, *176-177*, 678-686; b) P. Zhang, S. Kim, M. Fujitsuka, T. Majima, *Chem. Commun.,* **2017**; c) P. Zhang, T. Tachikawa, M. Fujitsuka, T. Majima, *Chem. Commun.,* **2015**, *51*, 7187-7190; d) E.-H. Kong, J. Lim, J. H. Lee, W. Choi, H. M. Jang, *Appl. Catal., B,* **2015**, *176-177*, 76-82.

[45] a) J. Pan, G. Liu, G. Q. Lu, H.-M. Cheng, *Angew. Chem., Int. Ed.,* **2011**, *50*, 2133-2137; b) T. R. Gordon, M. Cargnello, T. Paik, F. Mangolini, R. T. Weber, P. Fornasiero, C. B. Murray, *J. Am. Chem. Soc.,* **2012**, *134*, 6751-6761; c) T. Tachikawa, S. Yamashita, T. Majima, *J. Am. Chem. Soc.,* **2011**, *133*, 7197-7204; d) M. D'Arienzo, J. Carbajo, A. Bahamonde, M. Crippa, S. Polizzi, R. Scotti, L. Wahba, F. Morazzoni, *J. Am. Chem. Soc.,* **2011**, *133*, 17652-17661.

[46] a) T. Tachikawa, T. Majima, *Chem. Soc. Rev.,* **2010**, *39*, 4802-4819; b) T. Tachikawa, T. Majima, *Langmuir* **2012**, *28*, 8933-8943.

[47] a) M. W. Kanan, D. G. Nocera, *Science* **2008**, *321*, 1072-1075; b) M. W. Kanan, Y. Surendranath, D. G. Nocera, *Chem. Soc. Rev.,* **2009**, *38*, 109-114.

[48] a) R. S. Khnayzer, M. W. Mara, J. Huang, M. L. Shelby, L. X. Chen, F. N. Castellano, *ACS Cata.,* **2012**, *2*, 2150-2160; b) D. Liu, L. Jing, P. Luan, J. Tang, H. Fu, *ACS Appl. Mater. Inter.,* 2012, 5, 4046-4052.

[49] a) E. M. P. Steinmiller, K.-S. Choi, *Proc. Natl. Acad. Sci. U. S. A.* **2009**, *106*, 20633-20636; b) B. Klahr, S. Gimenez, F. Fabregat-Santiago, J. Bisquert, T. W. Hamann, *J. Am. Chem. Soc.,* **2012**, *134*, 16693-16700; c) D. K. Zhong, J. Sun, H. Inumaru, D. R. Gamelin, *J. Am. Chem. Soc.,* **2009**, *131*, 6086-6087; d) D. K. Zhong, D. R. Gamelin, *J. Am. Chem. Soc.,* **2010**, *132*, 4202-4207; e) D. K. Zhong, M. Cornuz, K. Sivula, M. Grätzel, D. R. Gamelin, *Energy Environ. Sci.,* **2011**, *4*, 1759-1764; f) K. J. McDonald, K.-S. Choi, *Chem. Mater.,* **2011**, *23*, 1686-1693; g) J. A. Seabold, K.-S. Choi, *Chem. Mater.,* **2011**, *23*, 1105-1112; h) D. Wang, R. Li, J. Zhu, J. Shi, J. Han, X. Zong, C. Li, *J. Phys. Chem. C,* **2012**, *116*, 5082-5089.

[50] a) S. Mann, *Nat. Mater.,* **2009**, *8*, 781-792; b) T. Tachikawa, P. Zhang, Z. Bian, T. Majima, *J. Mater. Chem. A* **2014**, *2*, 3381; c) Z. Nie, A. Petukhova, E. Kumacheva, *Nat. Nano.,* **2010**, *5*, 15-25; d) J.-W. Liu, H.-W. Liang, S.-H. Yu, *Chem. Rev.,* **2012**, *112*, 4770-4799.

[51] T. Tachikawa, M. Fujitsuka, T. Majima, *J. Phys. Chem. C,* **2007**, *111*, 5259-5275.

[52] a) Z. R. Yan, Q. F. Chen, P. Xia, W. X. Ma, B. S. Ren, *Nanotechnology* **2016**, *27*; b) T. H. Han, H. G. Wang, X. M. Zheng, *Rsc Adv.,* **2016**, *6*, 7829-7837.

[53] H. Imai, *J. Ceram. Soc. Jpn,* **2014**, *122*, 737-747.

[54] Q. Zhang, S. J. Liu, S. H. Yu, *J. Mater. Chem.* **2009**, *19*, 191-207.

[55] a) B. Liu, H. C. Zeng, *Chem. Mater.,* **2008**, *20*, 2711-2718; b) Y. Aoyama, Y. Oaki, R. Ise, H. Imai, *CrystEngComm* **2012**, *14*, 1405-1411.

[56] a) F. Colo, F. Bella, J. Nair, C. Gerbaldi, *J. Power Sources*, **2017**, *365*, 293-302; b) J. Nair, M. Destro, F. Bella, G. Appetecchi, C. Gerbaldi, *J. Power Sources*, **2016**, *306*, 258-267; c) L. Zolin, J. Nair, D. Beneventi, F. Bella, M. Destro, P. Jagdale, I. Cannavaro, A. Tagliaferro, D. Chaussy, F. Geobaldo, C. Gerbaldi, *Carbon*, **2016**, *107*, 811-822; d) L. Porcarelli, C. Gerbaldi, F. Bella, J. Nair, *Sci. Rep.*, **2016**, 6:19892; e) N. Nabilah, M. Radzir, S. Hanifah, A. Ahmad, N. Hassan, F. Bella, *J. Solid. State. Electr.*, **2015**, *19*, 3079-3085; f) E. Uchaker, G. Cao, *Nano Today* **2014**, *9*, 499-524; g) Y. Q. Liu, Y. Zhang, J. Wang, *CrystEngComm* **2014**, *16*, 5948-5967.

[57] X. X. Yao, X. H. Liu, T. Y. Liu, K. Wang, L. D. Lu, *CrystEngComm* **2013**, *15*, 10246-10254.

[58] H. G. Yang, G. Liu, S. Z. Qiao, C. H. Sun, Y. G. Jin, S. C. Smith, J. Zou, H. M. Cheng, G. Q. Lu, *J. Am. Chem. Soc.,* **2009**, *131*, 4078-4083.

[59] S. K. Choi, S. Kim, J. Ryu, S. K. Lim, H. Park, *Photochem. Photobiol. Sci.,* **2012**, *11*, 1437-1444.

[60] X. Yang, J. Qin, Y. Li, R. Zhang, H. Tang, *J. Hazard. Mater.,* **2013**, *261*, 342-350.

[61] S. Deng, V. Tjoa, H. M. Fan, H. R. Tan, D. C. Sayle, M. Olivo, S. Mhaisalkar, J. Wei, C. H. Sow, *J. Am. Chem. Soc.,* **2012**, *134*, 4905-4917.

[62] Z. Li, C.-K. Dong, J. Yang, S.-Z. Qiao, X.-W. Du, *J. Mater. Chem. A* **2016**, *4*, 2699-2704.

[63] a) Y. N. Guo, M. M. Gong, Y. S. Li, Y. L. Liu, X. C. Dou, *Nanoscale Res. Lett.,* **2016**, *11*; b) L. Zu, Y. Qin, J. Yang, *J. Mater. Chem. A* **2015**, *3*, 10209-10218.

[64] C. D. Gu, H. Zheng, X. L. Wang, J. P. Tu, *RSC Adv.,* **2015**, *5*, 9143-9153.

[65] a) J. P. Ge, Y. X. Hu, M. Biasini, W. P. Beyermann, Y. D. Yin, *Angew. Chem., Int. Ed.,* **2007**, *46*, 4342-4345; b) T. Lee, C. W. Zhang, *Pharm. Res.,* **2008**, *25*, 1563-1571; c) M. Kijima, Y. Oaki, H. Imai, *Chem. Eur. J.,* **2011**, *17*, 2828-2832.

[66] Y. Zhao, Y. Lu, Y. Hu, J. P. Li, L. A. Dong, L. N. Lin, S. H. Yu, *Small* **2010**, *6*, 2436-2442.

[67] L. Bergström, E. V. Sturm, G. Salazar-Alvarez, H. Cölfen, *Acc. Chem. Res.,* **2015**, *48*, 1391-1402.

[68] a) M. Agthe, E. Wetterskog, L. Bergstrom, *Langmuir* **2017**, *33*, 303-310; b) M. Agthe, T. S. Plivelic, A. Labrador, L. Bergstrom, G. Salazar-Alvarez, *Nano Lett.,* **2016**, *16*, 6838-6843.

[69] L. He, W. X. Que, *Appl. Mater. Today*, **2016**, *3*, 23-56.

[70] E. V. Sturm and H. Cölfen, *Chem. Soc. Rev.*, **2016**, *45*, 5821-5833.

[71] H. Imai, *Prog. Cryst. Growth Charact. Mater.*, **2016**, *62*, 212-226

Entry for the Table of Contents

MINIREVIEW

Mesocrystals with internal pores and anisotropic interfaces were developed for tuning superior properties in the wide applications related to the fields of energy harvesting, storage, and conversion.

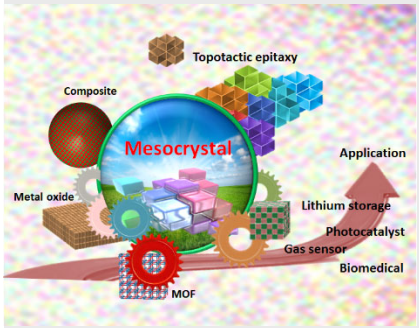

Peng Zhang, Takashi Tachikawa, Mamoru Fujitsuka and Tetsuro Majima**

Page No. – Page No.

The Development of Functional Mesocrystals for Energy Harvesting, Storage, and Conversion